Volume 3 | Number 1 | January 2018 | Pages 1–68

Nanoscale Horizons

The home for rapid reports of exceptional significance in nanoscience and nanotechnology

rsc.li/nanoscale-horizons

ISSN 2055-6756

ROYAL SOCIETY OF CHEMISTRY

COMMUNICATION

T. Saito, L. A. Berglund *et al.*

Nematic structuring of transparent and multifunctional nanocellulose papers

NCNST

Nanoscale Horizons

COMMUNICATION

View Article Online
View Journal | View Issue

Cite this: *Nanoscale Horiz.*, 2018, 3, 28

Received 21st July 2017,
Accepted 8th September 2017

DOI: 10.1039/c7nh00104e

rsc.li/nanoscale-horizons

Nematic structuring of transparent and multifunctional nanocellulose papers†

M. Zhao,[a] F. Ansari,[b] M. Takeuchi,[a] M. Shimizu,[a] T. Saito,*[a] L. A. Berglund*[b] and A. Isogai[a]

The nematic structuring of cellulose nanofibers (CNFs) is proposed as a nanostructural engineering tool for exploiting the potential of CNFs in conceptually new "transparent papers". The nematic-structured CNF papers exhibit superior mechanical properties, optical transparency, gas-barrier properties, heat transfer properties and electrical resistivity, compared with conventional randomly-structured CNF papers.

Conceptual insights

The conceptually new and sustainable "transparent papers" of wood cellulose nanofibers (CNFs) are characterized by exceptionally high strength, thermal expansion as low as for glasses, and superior gas-barrier properties, high thermal conductivity and electrical resistivity. Their possible applications thus range from structural members of energy, electronic, and sensing devices to direct uses as display panels and packaging materials. Here, the nematic structuring of CNFs is proposed as a nanostructural engineering tool for making full use of the potential of CNFs in transparent and multi-functional papers. We compare two types of macroscopically isotropic CNF papers with different nanofiber arrangements: one formed through evaporation condensation of nematic-ordered CNF dispersions with polydomain structure, and one through vacuum filtration of randomly-oriented CNF dispersion. Accordingly, the nematic-ordered CNF papers with densely-packed nanofiber arrangement exhibit superior mechanical properties, optical transparency, gas-barrier properties, heat transfer properties and electrical resistivity, compared with the conventional randomly-oriented CNF papers. The strategy proposed here for CNF arrangement is also applicable in the structuring of other one dimensional nanomaterials, such as carbon nanotubes, protein nanofibrils, and silver nanowires, for exploiting their potentials in macroscopically isotropic film structures.

Cellulose nanofibers (CNFs) are biobased, low-cost nanoscale fibrils with good mechanical properties.[1–3] The major resource of CNFs is wood. Wood is disintegrated into a pulp of tiny fibers by cooking, and the pulp is purified by bleaching. The fibers of bleached pulp are further finely disintegrated into CNFs. The wood pulp fiber, with a width of approximately 30 μm, consists of approximately ten billion 3 nm-wide cellulose fibrils, histologically defined as cellulose microfibrils.[4] These 3 nm-wide fibrils are mechanically strong and tightly bound in a pulp fiber, such that the tensile strength of single fibers (~1 GPa) is approximately twice that of some metals.[5,6] Disintegration of pulp fibers into CNFs was conventionally a high-energy consuming mechanical process, and the resulting CNFs were thick and heterogeneous in diameter (10–100 nm).[3,7] However, chemical or biochemical pretreatment of pulp overcame these problems.[8–14] One such pretreatment is 2,2,6,6-tetramethylpiperidinyl-1-oxyl (TEMPO)-mediated oxidation. This chemical reaction allows surface carboxylation of the 3 nm-wide cellulose fibrils in a pulp fiber. The carboxylate groups are dissociated in water, and electric double layer repulsion is induced between the assembled fibrils. Accordingly, these fibrils can be readily disintegrated from wood pulp and homogeneously dispersed as 3 nm-wide CNFs, through a mechanical process with low energy input.[8]

The low-energy production of fine and homogeneous CNFs opened up a new opportunity for nanotechnology. Large-scale production in industry is also underway. Recently, CNFs have often been compared to or combined with carbon nanotubes (CNTs).[1,15–17] CNTs are similar to CNFs in morphology and dimension and are already produced on an industrial scale although at a very high cost. Characteristics of both CNFs and CNTs include high mechanical strength. Although highly pure CNTs without defects exhibit very high strength estimated to be approximately 100 GPa,[18] mass-produced CNTs are not as strong.[19–21] Strength properties of CNFs and CNTs are indeed comparable in practical use (2–6 GPa).[22–24] CNFs exhibit some thermal conductivity but are electrically insulating,[25–27] whereas CNTs are both thermally and electrically conductive. The advantages of CNFs are their high dispersibility and hydrocolloidal stability.[28] Furthermore, it is easier to functionalize CNFs; the CNF surfaces bear reactive functional groups, such as hydroxyl and carboxyl groups.[29–32]

The potential of CNF-based materials can be illustrated by optically transparent films with high strength, thermal expansion

[a] *Department of Biomaterial Sciences, Graduate School of Agricultural and Life Sciences, The University of Tokyo, Tokyo 113-8657, Japan. E-mail: asaitot@mail.ecc.u-tokyo.ac.jp*
[b] *Wallenberg Wood Science Center and Department of Fibre and Polymer Technology, Royal Institute of Technology, SE-100 44 Stockholm, Sweden. E-mail: blund@kth.se*

† Electronic supplementary information (ESI) available: Experimental methods, Fig. S1–S3, and Tables S1 and S2. See DOI: 10.1039/c7nh00104e

as low as for glasses, and superior gas-barrier properties, high thermal conductivity and electrical resistivity.[33–37] These multi-functional CNF films have attracted attention as conceptually new "transparent papers".[36] Their possible applications range from structural members of energy, electronic, and sensing devices to direct uses as display panels and packaging materials.[38–45]

CNF films are prepared by drying colloidal water dispersions of CNFs. Although various film-preparation processes have been proposed, they can be broadly divided into two routes: CNF condensation by solvent evaporation or vacuum filtration of CNF dispersions.[33–37] The solvent evaporation is a slow process, and gradually enhances the interaction between dispersed CNFs during "condensation", whereas the vacuum filtration is a fast process, and dispersed CNFs are forced to deposit on filter membranes. Despite the fundamental differences in these CNF assembly routes, the resulting CNF films have similar multi-layered structures, where CNFs are packed almost parallel to each layer.[33,37] However, there are significant differences in the mechanical, optical, and gas barrier properties of these two types of films. One explanation for this contradiction is that the CNF materials in previous studies had different surface chemical structures, nanofiber diameters, and colloidal stabilities. Furthermore, their in-plane CNF arrangement, or how CNFs are packed in the plane direction of each layer, was not characterized. We have previously shown that CNFs are locally oriented and stacked in a plywood-like manner at the nanoscale when a film is prepared from a nematic-ordered dispersion of TEMPO-oxidized CNFs;[46] however, the material properties were not assessed.

Here, the nematic structuring of CNFs is proposed as a nanostructural engineering tool for making full use of the potential of CNFs in transparent and multi-functional films. We compare two types of CNF films with different in-plane structures: one formed through evaporation condensation of nematic-ordered CNF dispersions (Fig. 1a), and one through vacuum filtration of randomly-oriented CNF dispersions (Fig. 1b). Both films are composed of TEMPO-oxidized CNFs that are identical in chemical composition and morphology. The focus of the present work is to reveal the process-nanostructure and nanostructure–property relationships for isotropic CNF films. Thus, macroscopically oriented CNF films resulting from the stretching of vacuum-filtered wet CNF films, are not considered.[47,48]

The transmission electron microscopy (TEM) images of the cross-sections of the CNF films differed distinctly. The evaporation–condensed CNF films showed well-contrasted layered domains of uniaxially-oriented CNFs (Fig. 1c). In contrast, the vacuum-filtered CNF films had no such domains (Fig. 1d). The uniaxially-oriented CNFs in the evaporation-condensed films were also observed in scanning electron microscopy (SEM) images of the freeze-fractured surfaces of the films (Fig. 1e and f). Both films were composed of CNFs equally oriented parallel to the film plane (Fig. 1g–j); almost identical X-ray diffraction (XRD) patterns of short arc type were recorded upon irradiation of both film cross-sections (orientation index f of 87–89%), whereas a ring pattern was recorded for the out-of-plane direction. These microscopy and XRD-results indicate, (1) the evaporation–condensed films had a plywood-like nanostructure in which the layered domains of uniaxially-oriented CNFs were stacked parallel but still organized isotropically in-the-plane, resulting from averaging of the polydomain nematic arrangement of the CNFs, and (2) the vacuum-filtered films had a paper-like nanostructure in which CNFs were packed isotropically, randomly-in-the-plane but parallel to the plane, resulting from the forced deposition of randomly-dispersed CNFs onto a membrane filter. Although the oriented CNF domains in the evaporation-condensed films showed no clear boundary in the electron microscopy examination, their observable size was approximately 100–300 nm and 1–15 μm in the thickness and plane directions, respectively (Fig. S1, ESI†). The two types of CNF films prepared from the nematic-ordered and randomly-oriented dispersions, are hereafter abbreviated as NO and RO films, respectively.

Table 1 presents a summary of the structural profiles of the NO and RO films. The data were collected from typical films conditioned at 23 °C and 50% relative humidity (RH) after drying. The NO films were dried at 40 °C on a flat substrate through the evaporation–condensation process, while the RO films were also finally dried at 40 °C on a flat substrate after the vacuum-filtration process (see Experimental methods, ESI†). These two films had thicknesses of approximately 30 μm as measured using a micrometer, and their deviations were approximately 3% of each average thickness in the single films with planar dimensions of approximately 5×5 cm^2. The root-mean square roughness R_q values of the film surfaces, which were formed at the interfaces between wet CNFs and air in the drying processes, were small (less than 10 nm, ~0.03% of the film thickness) as determined by atomic force microscopy (AFM) for planar dimensions of 10×10 μm^2 (Fig. S2, ESI†). In fact, both the NO and RO films were flat and had smooth surfaces. However, there was a significant difference in the bulk density between the NO and RO films, even though they were prepared from the same CNF material. Thus, the bulk densities of the NO and RO films reflect their CNF-packing structure. The plywood-like CNF arrangement of the NO film can densely pack oriented CNFs, whereas the paper-like CNF arrangement of the RO film may induce porosity between the randomly-assembled CNFs (see the insets in Fig. 1c and d). Indeed, the RO films contained more moisture at 23 °C and 50% RH, and their porosities were almost twice as high as those of the NO films.

The most outstanding properties of CNF materials are their mechanical strength and modulus. An in-depth understanding of their mechanical properties is important from an application perspective.[49] Fig. 2 shows the uniaxial tensile properties of the two films. Both exhibited typical stress–strain behavior for CNF films (Fig. 2a);[33] a steep linear elastic region is observed at the initial strains, followed by yielding behavior at strains of approximately 1% and then a steady linear region of plastic deformation with strain hardening. However, distinct differences were observed for all the tensile properties of the NO and RO films (Table 2). The Young's modulus, yield stress, and tensile strength of the NO films were higher than those of the RO films. In particular, the yield stress of the NO films was

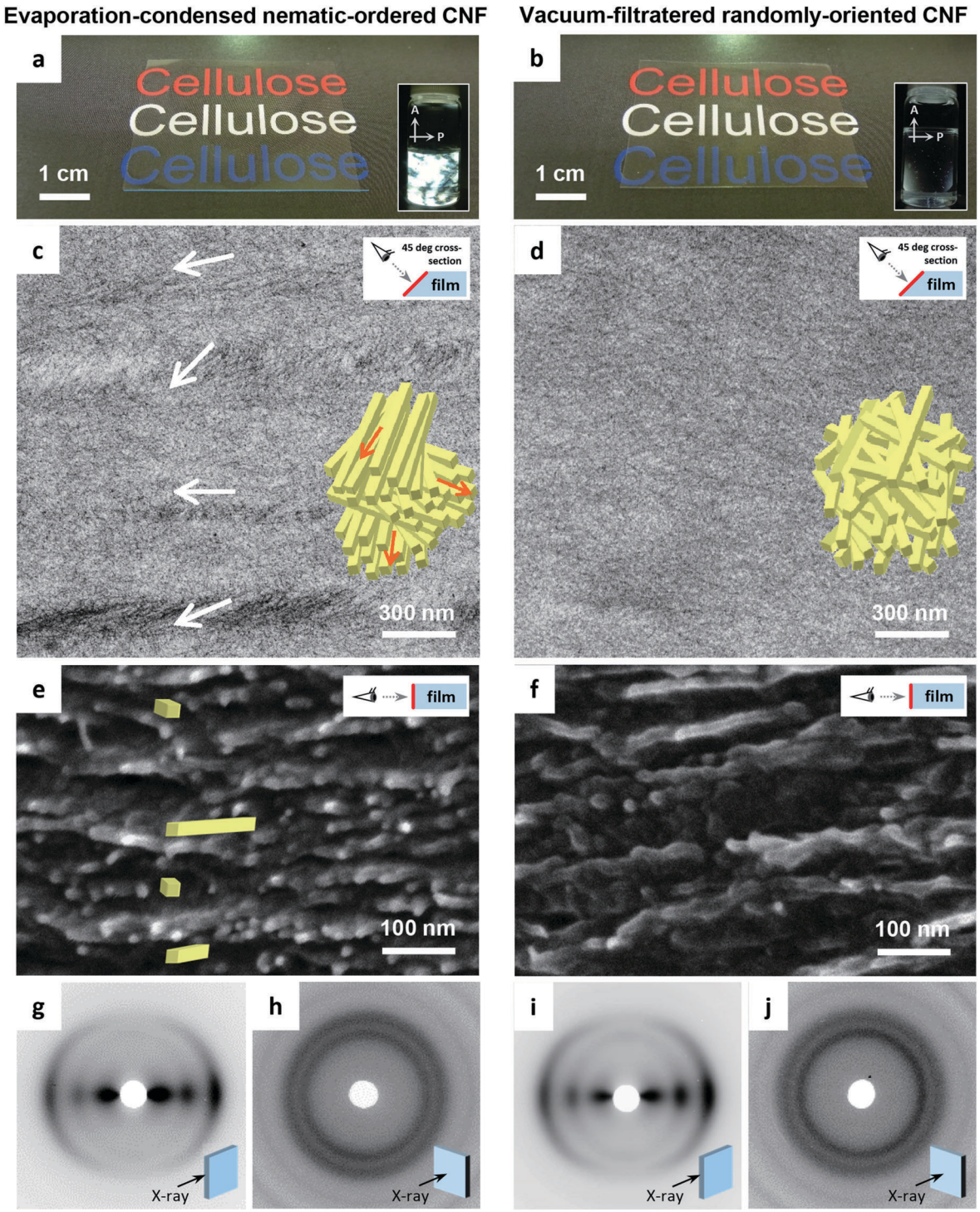

Fig. 1 Structure of CNF films. (a and b) Appearance of the evaporation–condensed and vacuum-filtered films. The insets show birefringence images of the 0.4% and 0.05% CNF dispersions used in the respective film preparation, indicating the polydomain-type nematic structuring of the CNFs in the 0.4% dispersion, and the isotropic structure of the randomly-oriented CNFs in the 0.05% dispersion. (c and d) TEM images of the 45° cross-sections of the films. (e and f) SEM images of the freeze-fractured surfaces of the films. (g–j) XRD diagrams of the films for the incident beam parallel or perpendicular to the film plane.

Table 1 Structural profiles of the films at 23 °C and 50% RH

Film type	Thickness (μm)	Surface roughness R_q (nm)	Bulk density (g cm^{-3})	Moisture content (%)	Porosity (%)
NO	28.3 ± 0.8	5.9 ± 2.5	1.54	9.2	9.7
RO	31.2 ± 1.0	8.6 ± 2.2	1.41	10.3	18.3

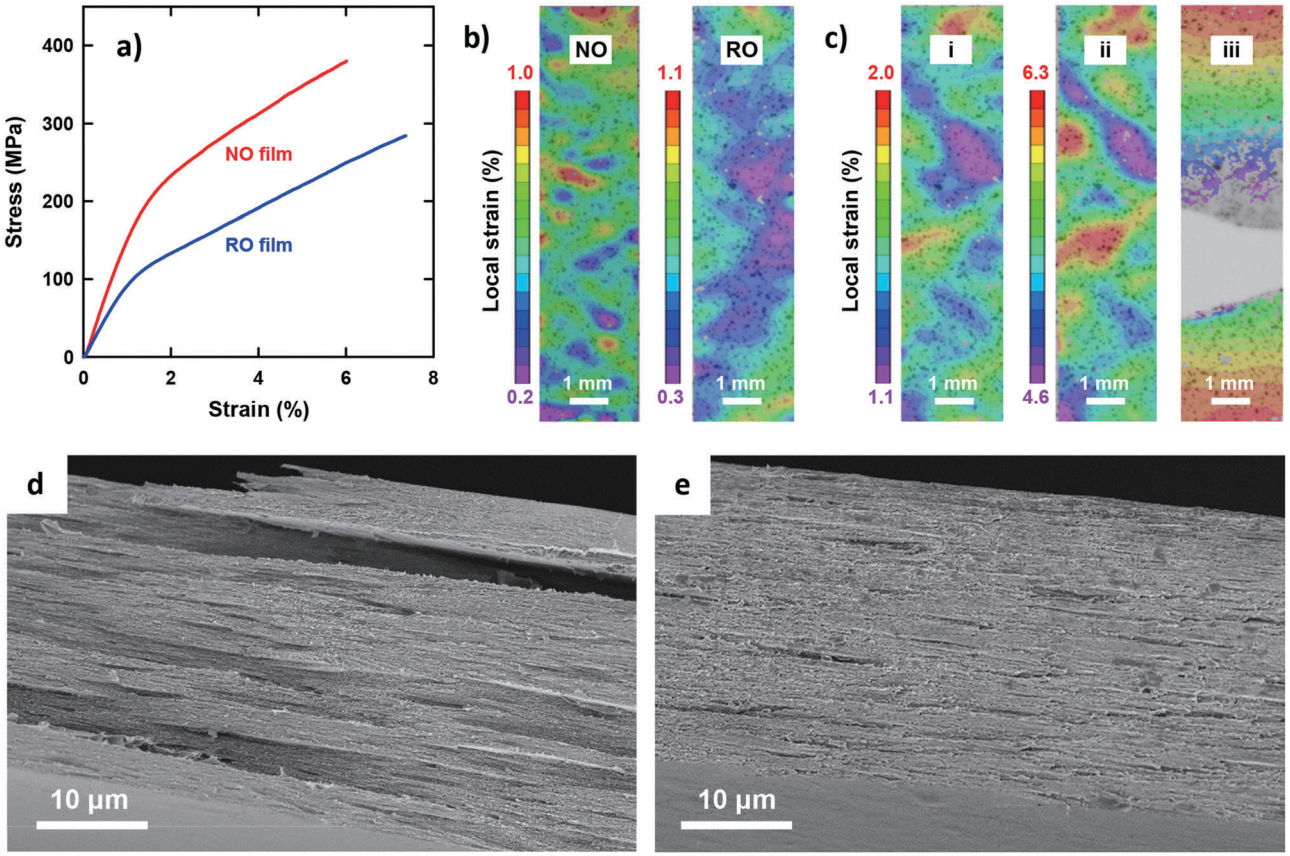

Fig. 2 Mechanical properties of the films. (a) Typical stress–strain curves. (b and c) In-plane strain fields on the tensile specimens determined by DIC analysis: (b) elastic deformation of NO and RO films at average strains of approximately 0.6%, and (c) plastic deformation of a RO film at average strains of (i) 1.6% and (ii) 5.5% and (iii) at break. SEM images of the tensile-fractured surfaces of the (d) NO and (e) RO films.

Table 2 Material properties of the films at 23 °C and 50% RH

	NO film	RO film
Tensile properties		
Young's modulus E (GPa)	15.4 ± 1.8	12.0 ± 0.5
Yield stress σ_y (MPa)	228 ± 0.2	117 ± 1.2
Tensile strength σ_b (MPa)	349 ± 46	259 ± 43
Elongation at break ε_b (%)	5.7 ± 0.4	6.6 ± 0.5
Light transmittance at 600 nm (%)	84.9 ± 0.7	74.3 ± 0.2
Oxygen gas permiability (mL μm m^{-2} day^{-1} kPa^{-1})	0.15	0.59
Heat transfer properties		
Diffusivity α (10^{-7} m^2 s^{-1})	1.03 ± 0.03	0.89 ± 0.07
Conductivity k (W m^{-1} K^{-1})	0.14 ± 0.01	0.11 ± 0.01
Electrical resistivity (10^8 Ω per square)	1.39 ± 0.13	0.93 ± 0.10

nearly twice as high as that of the RO films. These results can be explained by the dense CNF arrangement in the low-porosity NO films, which is in accordance with a previous report for the porosity dependency on tensile properties.[33] Yielding is associated with a local onset of separation or sliding of fibrils with respect to each other. Note that the RO films exhibited a higher elongation at break than the NO films, most likely because of lower stress levels because the nanofibers in the high-porosity RO films interacted more weakly and adsorbed more moisture. The network-like CNF structure of the RO films was thus able to deform to higher strains. The deformation mechanisms of the films were further investigated by analyzing the in-plane strain fields on the tensile specimens using a digital image correlation (DIC) system. At initial strains of approximately 0.6%, the RO films exhibited a more uniform strain field than the NO films (Fig. 2b). The heterogeneous strain field of the NO films even at low strain suggests that the degree of nematic ordering, or the degree of in-plane CNF orientation, varies by location within single NO films. The highly ordered CNFs interact strongly with each other in stiff regions of high stress transfer

efficiency during the initial stage, whereas the less ordered regions have lower stiffness and exhibit higher local strain. After yielding, the NO and RO films exhibited similar deformation behavior (Fig. 2c and Fig. S3, ESI†). The heterogeneity of the strain field was enhanced, and the high strain regions grew perpendicular to the tensile direction, resulting in ultimate fracture. The fracture appears to be initiated at the lateral edge of the specimens in regions of high local plastic strain.

The fractured surfaces of the two films differed significantly (Fig. 2d and e). The RO films exhibited fractured-surfaces that were flat and homogeneous on the microscale. In contrast, the NO films exhibited very rough fracture surfaces, showing pull-out fracture of large layered domains with planar sizes and thicknesses of the order of 10 μm and 1 μm, respectively. The large layered domains are assumed to be multiple-stacked structures of the thin layered units with thicknesses of approximately 100–300 nm based on the structural analyses in Fig. 1. These results indicate that shear yielding bands formed; local fracture initiated, and during crack growth, layered domains were pulled out from the surrounding material. The yielding and failure were most likely initiated in less ordered regions (see Fig. 2b). The final fracture appears to progress through fracture of thin sub-layer structures. The difference in the elongation at break between the NO and RO films was small but statistically significant, and should arise from the difference in deformation mechanisms and stress-levels between the plywood- and paper-like CNF arrangements.

The optical transparency of CNF films is attractive for their application as packaging materials and display panels. Fig. 3 presents the visible-light transmittance spectra of both films. Although both films are apparently transparent, the NO films exhibited higher transmittances than the RO films by approximately 10%. Note that the wet RO films obtained by vacuum filtration of the CNF dispersions were finally dried on a flat plastic plate in a similar manner as the NO films (see Experimental methods, ESI†); accordingly, there was no significant difference in the surface roughness of the films (see Table 1). Therefore, the higher transparency of the NO films can be explained solely by their lower porosity.

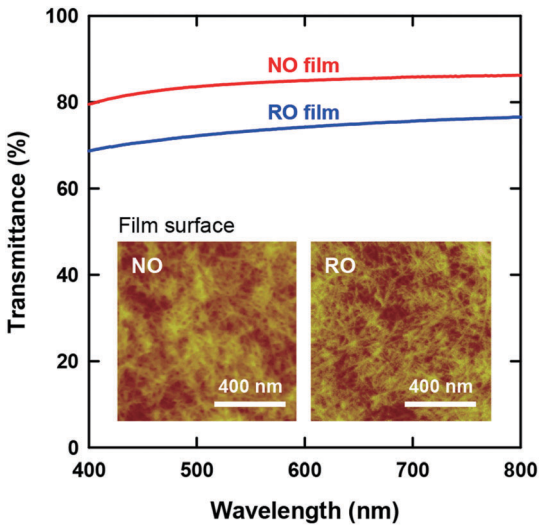

Fig. 3 Light transmittance spectra of the films. The insets show AFM images of the film surfaces.

The insets of Fig. 3 show the CNF arrangements at both film surfaces. As illustrated in Fig. 1, the internal structure of the NO films consisted of nematic-ordered CNFs. However, their surface CNFs were randomly oriented similar to those of the RO films. This phenomenon might be explained by the interference of nematic ordering by the interfacial force at the boundary between water dispersion and either air or a solid substrate. Similar disordering of ordered CNF structures at phase interfaces has also been observed in plant cell walls.[50]

One of the strong points of CNF films as packaging materials and display panels is their high oxygen gas-barrier property.[34,35,37] CNF films are assemblies of fibrous particles that strongly interact with each other *via* multiple hydrogen bonds as well as important weaker interactions. Gas permeation of CNF films is thus the diffusion of gas molecules through a highly constrained inter-nanofiber space. Therefore, it is reasonable that the NO films of low porosity exhibited lower oxygen gas permeability than the RO films (Table 2).

CNF films of low thermal expansion are attractive as substrates for flexible electronic devices.[36,40,42] In practical use of such devices, the substrates need good heat dissipation to reduce local heating as well as provide low thermal expansion.[25] We investigated the thermal diffusivity and conductivity of the two CNF films in the out-of-plane direction (Table 2). The NO films exhibited slightly higher diffusivities and conductivities than the RO films. Heat transfer within a CNF film is an intra- and inter-nanofiber phonon propagation, and the phonon scattering at the CNF interfaces significantly contributes to the thermal resistance.[26] Thus, CNF films with high density and low porosity should exhibit better heat-transfer properties. It is therefore reasonable that the low porosity NO films exhibited higher diffusivities and conductivities than the RO films. The higher Young's modulus of the NO films is also expected to correlate with the phonon propagation rate.

Electric insulation is required for many substrates in electronic devices.[27,42] Notably, in contrast to our expectation, the NO films exhibited higher electrical resistivity than the RO films (Table 2). The CNFs in the present study had sodium carboxylate groups on their surfaces, and thus, the conduction of Na ions present as counterions was assumed to contribute to the electric conductivity of the CNF films. The ion conduction within a CNF film needs moisture. Therefore, the lower electric resistivity of the RO films might be explained by their higher moisture content.

Another type of CNF films was prepared by vacuum filtration of nematic-ordered CNF dispersions. The resulting films had intermediate values in bulk density, moisture content, and porosity between NO and RO films, or the evaporation–condensed nematic-ordered CNF films, and the vacuum-filtered randomly-oriented CNF films (Tables S1, ESI†). Accordingly, the tensile properties, optical transparency, and gas permeability of the films were also intermediate between those of the NO and RO films (Tables S2, ESI†). These results suggest that the CNF arrangement in the films prepared by vacuum filtration of nematic-ordered CNF dispersions is intermediate between those of NO and RO films, or less ordered

but not randomly-oriented. This assumption is reasonable, considering that vacuum filtration forces the deposition of CNFs, whereas evaporation condensation is a slow process and enhances the ordering of the CNF dispersion of lyotropic nematics.

Conclusions

We compared two types of CNF films with different in-plane structures: NO films prepared by evaporative condensation of nematic-ordered CNF dispersions, and RO films prepared through vacuum filtration of randomly-oriented CNF dispersions. The NO films consisted of a plywood-like nanostructure with layered domains of uniaxially-oriented CNFs. The domain orientation angle varied, resulting in an overall isotropic in-plane arrangement as a film. In contrast, the RO films had a paper-like nanostructure in which CNFs were randomly packed in the plane at small scale but parallel to the plane. Although both the NO and RO films had flat and smooth surfaces, RO films had almost double the porosity of NO films, and showed significantly higher moisture content. Accordingly, the NO films with tightly packed CNF structure exhibited higher Young's modulus, yield stress, and tensile strength values but lower elongation at break than the RO films. Furthermore, the NO films exhibited superior optical transparency, gas-barrier properties and heat transfer properties compared with the RO films. The high porosity RO films were expected to exhibit higher electrical resistivity than the NO films; however, in fact, NO films exhibited higher resistivity. This result can be explained by the lower moisture content of the NO films. Vacuum filtration of nematic-ordered CNF dispersions was also performed, and the resulting CNF films were compared with the NO and RO films. Notably, the vacuum-filtered films of nematic-ordered CNFs exhibited intermediate properties between the NO and RO films, suggesting a less ordered but not randomly-oriented CNF arrangement in the plane direction of the vacuum-filtered films. Overall, the findings indicate that the nematic structuring of CNFs *via* evaporative condensation can function as a nanostructural engineering tool for exploiting the potential of CNFs in transparent and multifunctional films. This concept for nematic structuring of CNFs is also applicable in the structuring of other one dimensional nanomaterials, such as CNTs and silver nanowires.

Conflicts of interest

There are no conflicts to declare.

Acknowledgements

This study was partially supported by Grants-in-Aid for scientific research from the Japan Society for the Promotion of Science (15H04524 and 15K14765), the Core Research for Evolutional Science and Technology program (JPMJCR13B2) of the Japan Science and Technology Agency, and the Wallenberg Wood Science Center.

References

1 J. F. Beecher, *Nat. Nanotechnol.*, 2007, **2**, 466.
2 R. J. Moon, A. Martini, J. Nairn, J. Simonsen and J. Youngblood, *Chem. Soc. Rev.*, 2011, **40**, 3941.
3 D. Klemm, F. Kramer, S. Moritz, T. Lindstrom, M. Ankerfors, D. Gray and A. Dorris, *Angew. Chem., Int. Ed.*, 2011, **50**, 5438.
4 Y. Nishiyama, *J. Wood Sci.*, 2009, **55**, 241.
5 X. Li, L. G. Tabil and S. Panigrahi, *J. Polym. Environ.*, 2007, **15**, 25.
6 D. H. Page and F. Elhosseiny, *J. Pulp Pap. Sci.*, 1983, **84**, 99.
7 A. F. Turbak, F. W. Snyder and K. R. Sandberg, *J. Appl. Polym. Sci.*, 1983, **37**, 815.
8 T. Saito, Y. Nishiyama, J. L. Putaux, M. Vignon and A. Isogai, *Biomacromolecules*, 2006, **7**, 1687.
9 M. Henriksson, G. Henriksson, L. A. Berglund and T. Lindstrom, *Eur. Polym. J.*, 2007, **43**, 3434.
10 M. Paakko, M. Ankerfors, H. Kosonen, A. Nykanen, S. Ahola, M. Osterberg, J. Ruokolainen, J. Laine, P. T. Larsson, O. Ikkala and T. Lindstrom, *Biomacromolecules*, 2007, **8**, 1934.
11 L. Wagberg, G. Decher, M. Norgren, T. Lindstrom, M. Ankerfors and K. Axnas, *Langmuir*, 2008, **24**, 784.
12 H. Liimatainen, M. Visanko, J. A. Sirvio, O. E. O. Hormi and J. Niinimaki, *Biomacromolecules*, 2012, **13**, 1592.
13 M. Ghanadpour, F. Carosio, P. T. Larsson and L. Wagberg, *Biomacromolecules*, 2015, **16**, 3399.
14 Y. Noguchi, I. Homma and Y. Matsubara, *Cellulose*, 2017, **24**, 11.
15 S. Fujisawa, T. Saito, S. Kimura, T. Iwata and A. Isogai, *Compos. Sci. Technol.*, 2014, **90**, 96.
16 M. Wang, I. V. Anoshkin, A. G. Nasibulin, J. T. Korhonen, J. Seitsonen, J. Pere, E. I. Kauppinen, R. H. A. Ras and O. Ikkala, *Adv. Mater.*, 2013, **25**, 2428.
17 M. M. Hamedi, A. Hajian, A. B. Fall, K. Hakansson, M. Salajkova, F. Lundell, L. Wagberg and L. A. Berglund, *ACS Nano*, 2014, **8**, 2467.
18 B. Peng, M. Locascio, P. Zapol, S. Y. Li, S. L. Mielke, G. C. Schatz and H. D. Espinosa, *Nat. Nanotechnol.*, 2008, **3**, 626.
19 S. S. Xie, W. Z. Li, Z. W. Pan, B. H. Chang and L. F. Sun, *J. Phys. Chem. Solids*, 2000, **61**, 1153.
20 Y. Y. Huang, T. P. J. Knowles and E. M. Terentjev, *Adv. Mater.*, 2009, **21**, 3945.
21 T. V. Sreekumar, T. Liu, S. Kumar, L. M. Ericson, R. H. Hauge and R. E. Smalley, *Chem. Mater.*, 2003, **15**, 175.
22 T. Saito, R. Kuramae, J. Wohlert, L. A. Berglund and A. Isogai, *Biomacromolecules*, 2013, **14**, 248.
23 X. W. Wu, R. J. Moon and A. Martini, *Cellulose*, 2014, **21**, 2233.
24 K. M. O. Hakansson, A. B. Fall, F. Lundell, S. Yu, C. Krywka, S. V. Roth, G. Santoro, M. Kvick, L. P. Wittberg, L. Wagberg and L. D. Soderberg, *Nat. Commun.*, 2014, **5**, 4018.
25 K. Uetani, T. Okada and H. T. Oyama, *Biomacromolecules*, 2015, **16**, 2220.
26 J. A. Diaz, Z. J. Ye, X. W. Wu, A. L. Moore, R. J. Moon, A. Martini, D. J. Boday and J. P. Youngblood, *Biomacromolecules*, 2014, **15**, 4096.

27 U. Celano, K. Nagashima, H. Koga, M. Nogi, F. Zhuge, G. Meng, Y. He, J. De Boeck, M. Jurczak, W. Vandervorst and T. Yanagida, *NPG Asia Mater.*, 2016, **8**, e310.
28 A. B. Fall, S. B. Lindstrom, O. Sundman, L. Odberg and L. Wagberg, *Langmuir*, 2011, **27**, 11332.
29 R. K. Johnson, A. Zink-Sharp and W. G. Glasser, *Cellulose*, 2011, **18**, 1599.
30 S. Fujisawa, T. Saito, S. Kimura, T. Iwata and A. Isogai, *Biomacromolecules*, 2013, **14**, 1541.
31 H. Tang, N. Butchosa and Q. Zhou, *Adv. Mater.*, 2015, **27**, 2070.
32 J. R. McKee, E. A. Appel, J. Seitsonen, E. Kontturi, O. A. Scherman and O. Ikkala, *Adv. Funct. Mater.*, 2014, **24**, 2706.
33 M. Henriksson, L. A. Berglund, P. Isaksson, T. Lindstrom and T. Nishino, *Biomacromolecules*, 2008, **9**, 1579.
34 K. Syverud and P. Stenius, *Cellulose*, 2009, **16**, 75.
35 H. Fukuzumi, T. Saito, T. Iwata, Y. Kumamoto and A. Isogai, *Biomacromolecules*, 2009, **10**, 162.
36 M. Nogi, S. Iwamoto, A. N. Nakagaito and H. Yano, *Adv. Mater.*, 2009, **21**, 1595.
37 C. Aulin, M. Gallstedt and T. Lindstrom, *Cellulose*, 2010, **17**, 559.
38 G. Nystrom, A. Razaq, M. Stromme, L. Nyholm and A. Mihranyan, *Nano Lett.*, 2009, **9**, 3635.
39 R. Weishaupt, G. Siqueira, M. Schubert, M. M. Kampf, T. Zimmermann, K. Maniura-Weber and G. Faccio, *Adv. Funct. Mater.*, 2017, **27**, 1604291.
40 W. B. Kang, M. F. Lin, J. W. Chen and P. S. Lee, *Small*, 2016, **12**, 6370.
41 T. Inui, H. Koga, M. Nogi, N. Komoda and K. Suganuma, *Adv. Mater.*, 2015, **27**, 1112.
42 Y. Fujisaki, H. Koga, Y. Nakajima, M. Nakata, H. Tsuji, T. Yamamoto, T. Kurita, M. Nogi and N. Shimidzu, *Adv. Funct. Mater.*, 2014, **24**, 1657.
43 Z. Wang, P. Tammela, M. Strømme and L. Nyholm, *Adv. Energy Mater.*, 2017, DOI: 10.1002/aenm.201700130.
44 Y. Zhang, L. Li, L. Zhang, S. Ge, M. Yan and J. Yu, *Nano Energy*, 2017, **31**, 174.
45 F. Lai, Y.-E. Miao, Y. Huang, Y. Zhang and T. Liu, *ACS Appl. Mater. Interfaces*, 2016, **8**, 3558.
46 T. Saito, T. Uematsu, S. Kimura, T. Enomae and A. Isogai, *Soft Matter*, 2011, **7**, 8804.
47 H. Sehaqui, N. E. Mushi, S. Morimune, M. Salajkova, T. Nishino and L. A. Berglund, *ACS Appl. Mater. Interfaces*, 2012, 4, 1043.
48 C. Baez, J. Considine and R. Rowlands, *Cellulose*, 2014, **21**, 347.
49 A. J. Benítez and A. Walther, *J. Mater. Chem. A*, 2017, **5**, 16003.
50 J. C. Roland, D. Reis and B. Vian, *Tissue Cell*, 1992, **24**, 335.

